Recommendations for research and development

Future research and development activities should be directed by strategic choices, involving available resources, future applications and patent positions.

Further miniaturization of the catheter (≤ 1 mm OD) would enable investigation deeper into the arterial system. Especially the coronary application would benefit from such a development.

The current flexible drive-shafts perform adequately, but in future higher demands to accurate depiction of blood-vessel cross-sections may be made, possibly related to new methods of material and tissue characterization, based on the echo-information.
Also a change of working conditions may decrease the angular fidelity of the flex-shaft rotation transmission. In a hybrid catheter, for instance, suited for US-imaging as well as spark-erosion or mechanical drilling, mechanical power is required at the catheter-tip, most likely to be delivered by the same drive-shaft. Furthermore, ongoing miniaturization will change the properties of the flex-shaft. These arguments may show the importance of further optimization of the flex-shaft properties, along the guide-lines set in this thesis. Acquiring more understanding of the mechanics of the double-layer spiral itself would greatly support these investigations. The relationship between its construction parameters like the lead angle, the number of parallel filaments per layer, the interference force between the layers, the wire properties, etc., and the favourable qualities of the flex-shaft should be studied.

Incorporation of a micro-motor in the catheter-tip has started already and will hopefully yield a reliable scanning system, insensitive to catheter curvature. The driving motor in the driving unit, to which the catheter is connected, will become obsolete, so that the unit can become smaller and handier, serving bed-side ergonomics.
Down-scaling of the catheter to sizes ≤ 1 mm OD requires the development of a smaller micro-motor. This seems to be possible, applying the same principles, but will take a considerable research and development effort.

For other medical applications, like in urology or gynaecology, US-imaging catheters may also prove to be useful. Most likely the system will have to be modified to adapt to different medical demands. Application of other ultrasonic frequencies and the change of size and shape of the catheter/probe will probably be required.

The development of hybrid catheters, integrating US-imaging with an interventional method e.g. balloon dilation will enable the physician to investigate a stenosis, take

therapeutic measures and examine the result, all with the same catheter. It would save time and the image-plane would more accurately coincide with the site of intervention, than can be achieved with separate imaging and interventional catheters.

For the signal- and image-processing, obvious changes connected with the catheter development have to be made, but more independently efforts can be made to improve software ergonomics and software tools for image analysis, including 3-dimensional computer reconstruction of a section of a blood-vessel.

APPENDIX A String pulley driving mechanism

An introduction to this concept is given in § 3.2.2, together with a structure of the mechanism in Fig. 3.2-4. In this appendix some aspects of the method will be discussed in more detail and it will be shown that some major functional and constructive problems are to be solved when pursuing this method.

The success of the method would lie in the ability to accurately derive the tip-rotation angle from the linear string travel, monitored at the proximal end of the catheter.
Changes in tensile forces in the string ends as well as in the catheter-tube cause variations in the proximal string travel, which will be interpreted as corresponding with a certain tip-rotation angle, but actually are the result of changes in strain of the string and catheter-tube.

Because of the small diameter of the friction wheel, the system is sensitive to this problem. As an example the following reasoning and calculations are presented.

The dimensions of the catheter limit the diameter D of the friction wheel to about 1 mm. One degree of rotation corresponds therefore with 9 μm of travel of the string.

The string should be axially stiff, but very flexible. A thin, multi-fiber composed cable of e.g. Kevlar or carbon meets these requirements. The outer diameter of the string is limited to about 0.1 mm. The Young's modulus of Kevlar is 130.000 N/mm^2 and of carbon fiber up to 400.000 N/mm^2. Carbon fiber, however, is brittle, so it is doubtful whether a radius of curvature of 0.5 mm over the friction wheel is attainable for this fiber. The variation in length Δl of the Kevlar string under a variation of tensile force ΔF is given by:

$$\Delta l = \frac{\Delta F l}{EA} \qquad \text{(A-1)}$$

where
ΔF [N] = variation of tensile force
l [mm] = length
E [N/mm^2] = Young's modulus
A [mm^2] = cross-sectional area
EA [N] = axial stiffness

The Kevlar string of 2 m length (catheter length of 1 m) will elongate about 20 μm at an increase of the tensile force of 0.01 N (≈ 1 gf).

Analogously the change of the catheter length can be found, when variations of the axial force occur. The catheter, e.g. a polyethylene tube of 1.37 mm OD and 1.09 mm ID and a bending rigidity of about 30 Nmm^2, has an axial stiffness EA of about 160 N. A variation of the axial force of 0.01 N (≈ 1 gf) changes the length L of this catheter of 1 m length, with $\Delta L = 60$ μm.

The tip-rotation error angle γ [°] is given by:

$$\gamma = \frac{360(\Delta l + \Delta L)}{\pi D} \qquad \text{(A-2)}$$

An estimation of the tensile force in the string and the compression force in the catheter and their variations in a functional situation can be made, based on the fact that friction forces should be exceeded. Friction between the string and the catheter-tube is increased by the curved situation in which the catheter should function. The friction force $F_w = F_2 - F_1$ in one bend is ruled by the equation [1]:

$$F_2 = e^{\mu\varphi} F_1 \qquad \text{(A-3)}$$

where
F_1 [N] = ingoing tensile string force
F_2 [N] = outgoing tensile string force
μ = friction coefficient between string and catheter-tube
φ [rad] = angle of contact in the bend

The geometry of the catheter, following the tortuous pathway to the coronary arteries can roughly be approximated by 5 times a 90° curve: the introduction curve, the aortic arch (≈ 180°), the entrance into the coronary and the summation of other curves.

If the proximal string tensile force of the ingoing end of the string is F_{in} and the tensile force of the driven, outgoing end is F_{out} we find for the relationship between these two:

$$F_{out} = e^{5\pi\mu} F_{in} \qquad \text{(A-4)}$$

and for their variations:

$$\Delta F_{out} = e^{5\pi\mu} \Delta F_{in} \qquad \text{(A-5)}$$

The average tensile force $F_{s,\,av}$ in the string and its variation $\Delta F_{s,\,av}$ can be approximated by:

$$F_{s,\,av} = F_{tip} = e^{\frac{5\pi\mu}{2}} F_{in} \qquad \text{(A-6)}$$

and

$$\Delta F_{s,\,av} = \Delta F_{tip} = e^{\frac{5\pi\mu}{2}} \Delta F_{in} \qquad \text{(A-7)}$$

where F_{tip} is the tensile force in the driving string at the catheter-tip and ΔF_{tip} its variation.

The tensile forces in the two string ends at every catheter cross-section determine the compressive force in catheter-tube at that location. The average compressive force $F_{c,av}$ and its variation
$\Delta F_{c,av}$ can be estimated by:

$$F_{c,av} \approx -2F_{tip} = -2e^{\frac{5\pi\mu}{2}} F_{in} \qquad \text{(A-8)}$$

and

$$\Delta F_{c,av} \approx -2\Delta F_{tip} = -2e^{\frac{5\pi\mu}{2}} \Delta F_{in} \qquad \text{(A-9)}$$

The force F_{in} should be kept as small as possible, not to let $F_{c,av}$ grow too much. But F_{in} should have a certain minimum value to ensure enough string tension over the friction wheel in the tip to avoid slip. Furthermore this minimum value should be kept as constant as possible, to avoid increased fluctuations of the tensile force in the string and in the compressive force in the catheter tube. It will show to be difficult to stabilize very small pre-tensions F_{in}. We assume that F_{in} can be stabilized to variations ΔF_{in}. F_{out} and F_{tip} can be calculated, using respectively eqs. A-4 and A-6. The tip-error angle γ, due to the variations ΔF_{in}, can be estimated using eqs. A-1 and A-2, where the variation of the tensile force in the string $\Delta F_{s,av}$ is given by eq. A-7 and the variation of the compressive force in the catheter $\Delta F_{c,av}$ by eq. A-9. Some calculations have been performed for different values of the friction coefficient μ, F_{in} and ΔF_{in} (Table A-1).
The friction coefficient is not known exactly and may be reduced by using special materials or lubricants.

Table A-1 F_{out} *and* γ *as a function of* F_{in}, ΔF_{in} *and* μ.

μ	F_{in} [N]	ΔF_{in} [N]	F_{out} [N]	γ [°]
0.05	0.01	0.001	0.02	2.5
		0.01	0.02	24.5
	0.1	0.001	0.22	2.5
		0.01	0.22	24.5
0.1	0.01	0.001	0.05	3.6
		0.01	0.05	36.3
	0.1	0.001	0.48	3.6
		0.01	0.48	36.3
0.2	0.01	0.001	0.23	8.0
		0.01	0.23	79.7
	0.1	0.001	2.31	8.0
		0.01	2.31	79.7

This table shows that μ and ΔF_{in} should be kept very low (respectively < 0.05 and < 0.001 N), otherwise the variations in the tensile forces will cause large tip-rotation error angles.

A miniature gearing in the catheter-tip reducing the rotary speed by e.g. a factor 10 can solve the described problems because the tip-rotation error will be less sensitive to variations in length of the driving wire or catheter-tube. Needless to say that the development of this miniature speed-reduction device represents a technological problem by itself.

Another reason to keep the value of F_{in} low is to avoid the accumulation of the tensile force over the length of the string to high values, between the ingoing and the outgoing side. The string is also axially moving, so that the risk of damage to the polymer wall of the catheter becomes apparent. A stainless steel spiral, incorporated in the catheter-tube wall may be applied to reduce this risk.

If the string is situated (slightly) eccentrically in the catheter and its tension is high, a considerable bending moment can be developed, which causes unwanted catheter curvature.

Reference

1. Meriam J.L., Statics, SI version, John Wiley & Sons, Inc., New York, London, Sydney, Toronto, pp. 256-258, 1975.

APPENDIX B Effect of $EI_{\bar{y}} \neq EI_{\bar{z}}$ and pre-curvature on the rotation transmission characteristics of a flexible drive-shaft; analytical modelling

For the explanation of symbols, used in this appendix, see the list of symbols at the beginning of Chapter 4.
The analytical modelling in this appendix is based on the fluctuating strain energy content of the drive-shaft during rotation, due to $EI_{\bar{y}} \neq EI_{\bar{z}}$ or pre-curvature. Before presenting these models, a description is given of unsymmetrical bending, torsion and strain energy of the shaft.

Unsymmetrical bending

A local Cartesian coordinate system is defined on the drive-shaft (Fig. B-1). The curve in the drive-shaft, with constant curvature, is restricted to the xz-plane by the catheter-tube through which it runs (Fig. 4.1-1). The x-axis coincides with the local central axis of the drive-shaft.

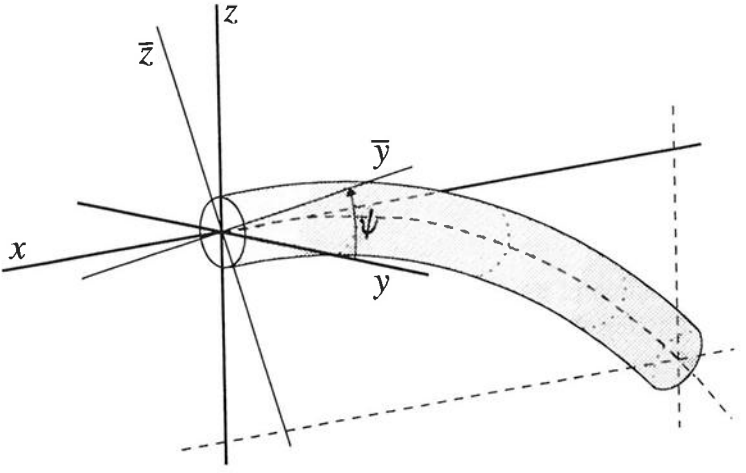

Fig. B-1 Definition of local xyz-axes on a drive-shaft cross-section and the principal axes of bending $\bar{y}$ and $\bar{z}$.

We assume that the drive-shaft cross-section has two perpendicular axes of symmetry, so that the two principal axes of bending, $\bar{y}$ and $\bar{z}$, can be defined. The $\bar{y}$- and $\bar{z}$-axis are rotated around the x-axis over an angle ψ with respect to the y- and z-axis.

For the bending moments $M_{\bar{y}}$ and $M_{\bar{z}}$ in the principal directions we find [1, p. 296]:

$$M_{\bar{y}} = - \kappa_{\bar{z}} EI_{\bar{y}} \tag{B-1}$$

and

$$M_{\bar{z}} = \kappa_{\bar{y}} EI_{\bar{z}} \tag{B-2}$$

where
$\kappa_{\bar{y}}$, $\kappa_{\bar{z}}$ is the curvature in $\bar{y}$ and $\bar{z}$ direction
$EI_{\bar{y}}$, $EI_{\bar{z}}$ is the bending rigidity when bending around respectively the $\bar{y}$- and $\bar{z}$-axis

For the curvatures $\kappa_{\bar{y}}$ and $\kappa_{\bar{z}}$ we find:

$$\kappa_{\bar{y}} = \kappa_y \cos\psi + \kappa_z \sin\psi \tag{B-3}$$

and

$$\kappa_{\bar{z}} = \kappa_z \cos\psi - \kappa_y \sin\psi \tag{B-4}$$

The confinement of the shaft in the *xz*-plane means that $\kappa_y = 0$ and $\kappa_z = \kappa_1 = 1/\rho_1$, so that:

$$M_{\bar{y}} = - \frac{EI_{\bar{y}} \cos\psi}{\rho_1} \tag{B-5}$$

and

$$M_{\bar{z}} = \frac{EI_{\bar{z}} \sin\psi}{\rho_1} \tag{B-6}$$

Torsion

An infinitesimal section of the curved drive-shaft is also twisted by a torque M_t, causing a torsion angle $d\eta$ (Fig. B-2). For the specific torsion angle χ we find:

$$\chi = \frac{d\eta}{ds} = \frac{M_t}{S_t} \tag{B-7}$$

where
S_t = torsional rigidity of the drive-shaft

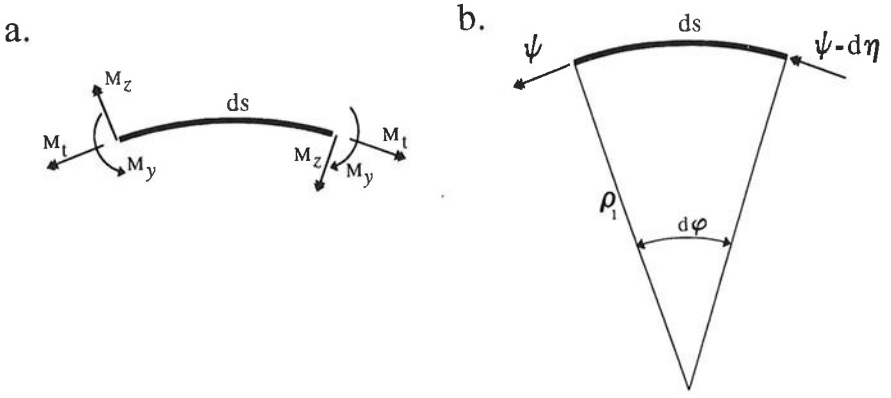

Fig. B-2 Curved section of drive-shaft, with bending moments and torques (a) and deformation (b). In case of unsymmetrical bending a moment M_z can occur, although the curve remains situated in the xz-plane. Note that the rotation error angle θ, caused by torsion of the drive-shaft, is equal to -η.

Strain energy of the drive-shaft

The strain energy content W_{str} of a curved and torqued shaft, with total length L is:

$$W_{str} = W_b + W_t = \int_0^L \{ \int_0^{\kappa_{\bar{z}}} -M_{\bar{y}}\, d\kappa'_{\bar{z}} + \int_0^{\kappa_{\bar{y}}} M_{\bar{z}}\, d\kappa'_{\bar{y}} + \int_0^{\chi} M_t\, d\chi' \}\, ds \quad \text{(B-8)}$$

where W_b and W_t are respectively the strain energies of the shaft due to bending and torsion.
Integration over $\kappa_{\bar{z}}$, $\kappa_{\bar{y}}$ and χ renders:

$$W_{str} = \int_0^L \{ \frac{EI_{\bar{y}}\, \kappa_{\bar{z}}^2}{2} + \frac{EI_{\bar{z}}\, \kappa_{\bar{y}}^2}{2} + \frac{S_t \chi^2}{2} \}\, ds \quad \text{(B-9)}$$

and considering eqs. B-1, B-2, B-5, B-6 and B-7 this results in:

$$W_{str} = \int_0^L \{ \frac{EI_{\bar{y}} \cos^2\psi + EI_{\bar{z}} \sin^2\psi}{2\rho_1^2} + \frac{S_t\, \chi^2}{2} \}\, ds \quad \text{(B-10)}$$

The infinitesimal work performed on the drive-shaft by external forces and moments is

equal to the change of strain energy and internal dissipation:

$$T\,d\psi_1 - dW_{f,out} = dW_b + dW_t + dW_{f,in} \qquad \text{(B-11)}$$

where
T = external torque
ψ_1 = proximal rotation angle
$W_{f,out}$ = external friction losses
$W_{f,in}$ = internal dissipation

The rotation error angle θ can be found from:

$$\theta = -\int_0^L \chi\, ds = -\int_0^L \frac{M_t}{S_t}\, ds \qquad \text{(B-12)}$$

Unequal bending rigidity in different bending planes: $EI_{\bar{y}} \neq EI_z$

First approximation model
For the simple drive-shaft geometry, as given in Fig. 4.1-1 and under the assumption that $l_1 >> s_1$, the rotation error angle θ can be approximated by:

$$\theta \approx \psi_2 - \psi_1 \qquad \text{(B-13)}$$

This way the torsion angle in the curved section s_1 is neglected relative to the torsion angle in the straight section l_1. If we assume that the absolute value of the torsion angle in the curved section is also small, we can define for this section $S_t = \infty$, $\chi = 0$ and the rotation angle $\psi = \psi_2$. Over the straight length l_1 the torque T is constant and $\chi = \eta/l_1 = -\theta/l_1$. If friction losses are not taken into account, the combination of eqs. B-10 and B-11 gives:

$$T = \frac{d}{d\psi_1}\int_0^{s_1} \frac{EI_{\bar{y}}\cos^2\psi_2 + EI_z \sin^2\psi_2}{2\rho_1^2}\, ds + \frac{d}{d\psi_1}\left(\frac{T^2 l_1}{2S_t}\right) \qquad \text{(B-14)}$$

Taking into account eq. B-13 we get:

$$T = \frac{s_1}{2\rho_1^2}\left(1 + \frac{d\theta}{d\psi_1}\right)\{EI_z - EI_{\bar{y}}\}\sin 2\psi_2 - T\frac{d\theta}{d\psi_1} \qquad \text{(B-15)}$$

so that:

$$T = \frac{s_1}{2\rho_1^2}(EI_{\bar{z}} - EI_{\bar{y}})\sin 2\psi_2 \qquad \text{(B-16)}$$

For a uniformly driven drive-shaft, we find that $\psi_1 = \omega t$ where ω is the angular velocity and t is the time, so that substitution in eq. B-13 gives:

$$\psi_2 = \omega t + \theta \qquad \text{(B-17)}$$

The approximated rotation error angle $\theta = -\eta$ over the whole shaft is given by:

$$\theta = \psi_{dist} - \psi_{prox} \approx \psi_2 - \psi_1 = -\frac{Tl_1}{S_t} = -\frac{s_1 l_1 p\overline{EI}}{\rho_1^2 S_t}\sin(2(\omega t+\theta)) \qquad \text{(B-18)}$$

and for a drive-shaft curve angle $\varphi_1 = \pi/2$:

$$\theta \approx -\frac{\pi l_1 p\overline{EI}}{2\rho_1 S_t}\sin(2(\omega t+\theta)) \qquad \text{(B-18a)}$$

where:

$$\overline{EI} = \frac{(EI_{\bar{y}} + EI_{\bar{z}})}{2} \quad , \quad p = \frac{(EI_{\bar{z}} - EI_{\bar{y}})}{(EI_{\bar{y}} + EI_{\bar{z}})} \qquad \text{(B-19)}$$

and p is small for a good quality drive-shaft.

Improved model

If the assumption $l_1 >> s_1$ is not valid, torsion in the curved section cannot be disregarded in comparison with the torsion in the straight section. Also in case the absolute value of the torsion angle in the curved section is not small this angle has to be taken into account. That means for the curved section $S_t \neq \infty$ and the rotation angle in this section is ψ.

The torque T is caused by the changing strain energy in the curved section. Along the curve the torque M_t will decrease until it is zero at the distal tip. A good approximation can be made by assuming a linear decline of the torque M_t, so that $M_t = T$ for $s = 0$ and

$M_t = 0$ at the distal tip, where $s = s_1$:

$$M_t = T\,(1 - \frac{s}{s_1}) \tag{B-20}$$

and according to eq. B-7 the specific torsion angle χ then is:

$$\chi(s) = \frac{T}{S_t}\,(1 - \frac{s}{s_1}) \tag{B-21}$$

The rotation error angle θ_s in this section, relative to the rotation angle ψ_2 is:

$$\theta_s = \psi - \psi_2 = -\int_0^s \chi(s')\,ds' = -\frac{T}{S_t}(s - \frac{s^2}{2s_1}) \tag{B-22}$$

Disregarding friction losses, eqs. B-10 and B-11 give:

$$T = \frac{d}{d\psi_1}\int_0^{s_1}\{\frac{EI_{\bar{y}}\cos^2(\psi_2+\theta_s) + EI_{\bar{z}}\sin^2(\psi_2+\theta_s)}{2\rho_1^2} + \frac{S_t\,\chi^2}{2}\}ds + \frac{d}{d\psi_1}(\frac{T^2 l_1}{2S_t}) \tag{B-23}$$

Combined with eq. B-22 and under the assumption that θ_s is small enough to approximate: $\sin(2(\psi_2+\theta_s)) \approx \sin(2\psi_2) + 2\theta_s\cos(2\psi_2)$, we find:

$$T = \frac{p\overline{EI}s_1}{\rho_1^2}\,\sin\{\,2\psi_2 - \frac{2Ts_1}{3S_t}\,\} \tag{B-24}$$

and a better approximation of the torque $M_t(s)$ in the curve, than given by eq. B-20, will result from an iteration step:

$$M_t(s) = \frac{p\overline{EI}(s_1-s)}{\rho_1^2}\,\sin\{\,2\psi_2 - \frac{2T}{S_t}\,(\frac{s+s_1}{3} - \frac{s^2}{6s_1})\,\} \tag{B-25}$$

The rotation error angle θ_{t1} over the straight section can be derived from eq. B-24,

considering eqs. B-12 and B-13:

$$\theta_{l_1} = -\frac{s_1 l_1 p\overline{EI}}{\rho_1^2 S_t} \sin\{\, 2\omega t + 2(1+\frac{s_1}{3l_1})\theta_{l_1} \,\} \qquad \text{(B-26)}$$

and for a drive-shaft curve angle $\varphi_1 = \pi/2$:

$$\theta_{l_1} = -\frac{\pi l_1 p\overline{EI}}{2\rho_1 S_t} \sin\{\, 2\omega t + 2(1+\frac{s_1}{3l_1})\theta_{l_1} \,\} \qquad \text{(B-26a)}$$

The rotation error angle θ_{s1} over the whole curve can be found from integration of eq. B-25. The phase-shift at which the maximum error angle occurs is the same as in eq. B-26, because both maximum values of the rotation error angles θ_{l1} and θ_{s1} occur when T reaches its maximum value. So we find:

$$\theta_{s_1} = -\frac{s_1^2 p\overline{EI}}{2\rho_1^2 S_t} \sin\{\, 2\omega t + 2(1+\frac{s_1}{3l_1})\theta_{l_1} \,\} \qquad \text{(B-27)}$$

and for a drive-shaft curve angle $\varphi_1 = \pi/2$:

$$\theta_{s_1} = -\frac{\pi^2 p\overline{EI}}{8 S_t} \sin\{\, 2\omega t + 2(1+\frac{s_1}{3l_1})\theta_{l_1} \,\} \qquad \text{(B-27a)}$$

The value of the rotation error angle at the distal tip is:

$$\theta = \theta_{l_1} + \theta_{s_1} = -\frac{s_1 p\overline{EI}}{\rho_1^2 S_t}(l_1 + \frac{s_1}{2}) \sin\{\, 2\omega t + 2(1+\frac{s_1}{3l_1})\theta_{l_1} \,\} \qquad \text{(B-28)}$$

and for a drive-shaft curve angle $\varphi_1 = \pi/2$:

$$\theta = -\frac{\pi p\overline{EI}}{2 S_t}(\frac{l_1}{\rho_1} + \frac{\pi}{4}) \sin\{\, 2\omega t + 2(1+\frac{s_1}{3l_1})\theta_{l_1} \,\} \qquad \text{(B-28a)}$$

Drive-shaft pre-curvature

First approximation model

We still look at a drive-shaft in a catheter-tube, curved in the way as shown Fig. 4.1-1. Now the flexural rigidity is equal in all bending planes: $EI_{\bar{y}} = EI_{\bar{z}} = EI$ (Fig. B-1), but the part of the drive-shaft running through the curved section of the catheter tube ($\kappa = \kappa_1$ in z direction) has been given a pre-curvature $\kappa = \kappa_0$ in $\bar{z}$ direction. Again we assume that the rotation error angle $\theta \approx \psi_2 - \psi_1$, because the straight part $l_1 >> s_1$. No torsion angle over the curved section is taken into account; here S_t is supposed to be ∞ and the rotation angle $\psi = \psi_2$.

Eqs. B-3 and B-4 turn into:

$$\kappa_{\bar{y}} = \kappa_1 \sin\psi \tag{B-29}$$

and

$$\kappa_{\bar{z}} = \kappa_1 \cos\psi - \kappa_0 \tag{B-30}$$

The combination of eqs. B-9 and B-11 with eqs. B-29 and B-30 turns into:

$$T = \frac{d}{d\psi_1}\{\frac{EIs_1}{2}(\kappa_1^2 - 2\kappa_0\kappa_1\cos\psi_2 + \kappa_0^2)\} + \frac{d}{d\psi_1}(\frac{T^2 l_1}{2S_t}) =$$

$$= EI\kappa_0\kappa_1 s_1 (1 + \frac{d\theta}{d\psi_1}) \sin\psi_2 - T\frac{d\theta}{d\psi_1} \tag{B-31}$$

so that, with $\kappa_0 = 1/\rho_0$ and $\kappa_1 = 1/\rho_1$ we find for the torque T:

$$T = \frac{s_1 EI}{\rho_0\rho_1} \sin\psi_2 \tag{B-32}$$

and for the rotation error angle $\theta = -\eta$ we find after substitution of eq. B-17:

$$\theta = \psi_{dist} - \psi_{prox} \approx \psi_2 - \psi_1 = -\frac{Tl_1}{S_t} = -\frac{s_1 l_1 EI}{\rho_0\rho_1 S_t} \sin(\omega t + \theta) \tag{B-33}$$

and for a drive-shaft curve angle $\varphi_1 = \pi/2$:

$$\theta = -\frac{\pi l_1 EI}{2\rho_0 S_t} \sin(\omega t+\theta) \qquad \text{(B-33a)}$$

Improved model

Similar to the improved model for $EI_y \neq EI_z$, the improved model describing the rotation error angle due to pre-curvature should include the situation where $l_1 >> s_1$ is not valid. For the curved section $S_t \neq \infty$ and the rotation angle $\psi \neq \psi_2$. The rotation error angle θ_s over a length s of the curved section is defined by eq. B-22.

The analysis is analogous to the way the improved model for $EI_y \neq EI_z$ has been obtained.

The combination of eqs. B-9 and B-11 turns into:

$$T = \frac{d}{d\psi_1} \int_0^{s_1} \{\frac{EI}{2}(\kappa_1^2 - 2\kappa_0\kappa_1\cos(\psi_2+\theta_s) + \kappa_0^2) + \frac{S_t\chi^2}{2}\} ds + \frac{d}{d\psi_1}(\frac{T^2 l_1}{2S_t}) \qquad \text{(B-34)}$$

and θ_s is small enough to assume: $\cos(\psi_2+\theta_s) = \cos\psi_2 - \theta_s\sin\psi_2$.

The approximation model based on eq. B-20, B-21 and B-22 gives for the rotation error angle over the straight section of the shaft:

$$\theta_{l_1} = -\frac{s_1 l_1 EI}{\rho_0\rho_1 S_t} \sin\{\omega t + (1+\frac{s_1}{3l_1})\theta_{l_1}\} \qquad \text{(B-35)}$$

and for a drive-shaft curve angle $\varphi_1 = \pi/2$:

$$\theta_{l_1} = -\frac{\pi l_1 EI}{2\rho_0 S_t} \sin\{\omega t + (1+\frac{s_1}{3l_1})\theta_{l_1}\} \qquad \text{(B-35a)}$$

and the rotation error angle θ over the whole shaft:

$$\theta = \theta_{l_1} + \theta_{s_1} = -\frac{s_1 EI}{\rho_0\rho_1 S_t}(l_1 + \frac{s_1}{2}) \sin\{\omega t + (1+\frac{s_1}{3l_1})\theta_{l_1}\} \qquad \text{(B-36)}$$

and for a drive-shaft curve angle $\varphi_1 = \pi/2$:

$$\theta = -\frac{\pi EI}{2\rho_0 S_t}\left(l_1 + \frac{s_1}{2}\right) \sin\left\{\omega t + \left(1+\frac{s_1}{3l_1}\right)\theta_{l_1}\right\} \qquad \text{(B-36a)}$$

Reference

1. Timoshenko S.P., Gere J.M., Mechanics of Materials, Van Nostrand Reinhold Company, International Student Edition, 1973.

APPENDIX C Effect of friction on the rotation transmission characteristics of a flexible drive-shaft; analytical modelling

Two cases will be analysed:
1. A drive-shaft in a curved piece of tubing, with constant radius of curvature.
2. A drive-shaft in a curved piece of tubing, with a section of constant radius of curvature and two equal connecting straight ends.

Case 1

In Fig. C-1 a piece of tubing is shown, represented only by its two clearance boundaries (clearance = c) with respect to the drive-shaft, which is represented by its centre-line. The tube is bent over an angle φ_1, with radius ρ_{ib} of the inside bend and radius ρ_{ob} of the outside bend. The radius of curvature of the catheter centre-line is $\rho = (\rho_{ib}+\rho_{ob})/2$. The shaft interacts with the tube on (at least) three points. At the two ends of the tube the angle between the centre-lines of the drive-shaft and the catheter-tube is ξ.

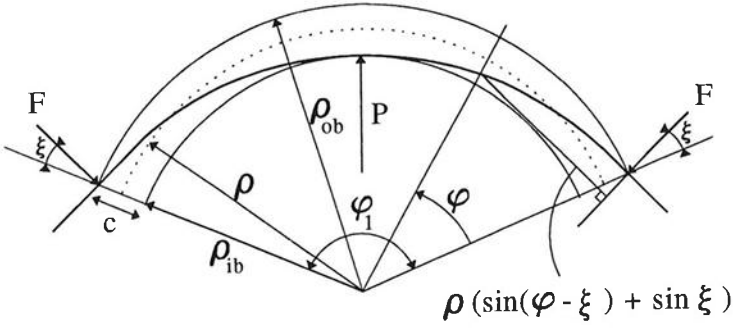

Fig. C-1 Drive-shaft in a curved piece of catheter tubing. The drive-shaft is represented by its centre-line, the tubing by its inner walls, the distance between which is the clearance.

The situation is symmetrical, so we study only one side of it. At the end of the tube its inner wall applies a force F to the drive-shaft. Some trigonometric analysis shows that the bending moment in the shaft, caused by F, at an angular position φ is:

$$M_\varphi = \frac{EI}{\rho_i} = F\,\rho\,(\sin(\varphi-\xi) + \sin\xi) \qquad \text{(C-1)}$$

where ρ_i is the radius of curvature of the drive-shaft.

If φ and ξ are small (justification of this assumption will follow), we get for ρ_i:

$$\rho_i = \frac{EI}{F\,\rho\,\varphi} \tag{C-2}$$

ρ_i decreases with increasing angle φ, until the shaft interacts with the inside bend of the tube inner wall at $\varphi = \beta$, where a second force F, in opposite direction, is applied to the shaft (Fig. C-2).

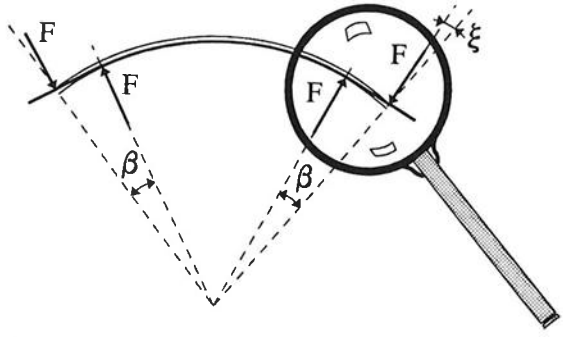

Fig. C-2 A second lateral force is applied to the drive-shaft at an angle $\varphi = \beta$.

If β is small, which will be shown to be generally the case, two sets of forces, working on the ends of the drive-shaft, act as two couples bringing about a constant bending moment M in the drive-shaft in the middle section and a radius of curvature close to ρ. That means:

$$M = F\,\beta\,\rho = \frac{EI}{\rho} \tag{C-3}$$

so that:

$$\beta = \frac{EI}{F\,\rho^2} \tag{C-4}$$

and combining eqs. C-2 and C-4 we find:

$$\rho_i = \frac{\beta}{\varphi}\,\rho \tag{C-5}$$

Between $\varphi = \beta$ and $\varphi = 0$ the radius of curvature ρ_i of the shaft increases from $\rho_i = \rho$ to $\rho_i = \infty$, while traversing from the inside bend to the outside bend (Fig. C-3).

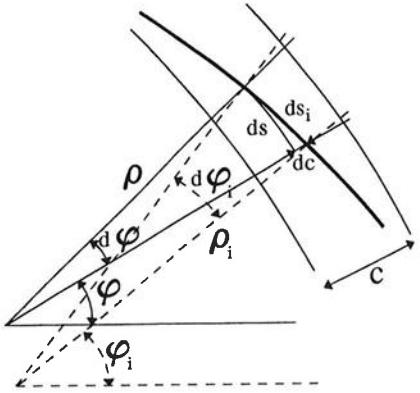

Fig. C-3 Detail of drive-shaft in catheter-tube for 0 < φ < β (Fig. C-2), with definition of infinitesimal geometrical quantities.

The relationship between the angle β and the clearance c can be found from Fig. C-3, where:

$$\left.\begin{aligned} \rho &= \frac{ds}{d\varphi} \\ \rho_i &= \frac{ds_i}{d\varphi_i} \end{aligned}\right\} \Rightarrow \rho_i = \rho\frac{d\varphi}{d\varphi_i} \qquad \text{(C-6)}$$

$$ds_i \approx ds$$

Elimination of ρ_i from eqs. C-5 and C-6 gives:

$$d\varphi_i = \frac{\varphi}{\beta} d\varphi \qquad \text{(C-7)}$$

Integration renders:

$$\varphi_i = \xi + \int_0^{\varphi} \frac{\varphi'}{\beta}\, d\varphi' = \xi + \frac{\varphi^2}{2\beta} \qquad \text{(C-8)}$$

For $\varphi \geq \beta$ the drive-shaft follows the inside bend, so that if $\varphi = \beta$ then also $\varphi_i = \beta$.

Substitution of this condition in eq. C-8 gives:

$$\xi = \frac{\beta}{2} \tag{C-9}$$

Combined with eq. C-8:

$$\varphi_i = \frac{\beta}{2} + \frac{\varphi^2}{2\beta} \tag{C-10}$$

The infinitesimal radial displacement of the drive-shaft between $\varphi = \beta$ and $\varphi = 0$ is:

$$dc = (\varphi_i - \varphi)\, ds = (\varphi_i - \varphi)\, \rho\, d\varphi \tag{C-11}$$

Substitution of eq. C-10 in eq. C-11 and integration for $\varphi = 0$ until $\varphi = \beta$ result in:

$$c = \frac{\rho\beta^2}{6} \quad \Rightarrow \quad \beta = \sqrt{\frac{6c}{\rho}} \tag{C-12}$$

Eq. C-12 shows that if $c/\rho < 0.02$, then $\beta < 0.35$ rad (= 20 °). In most practical situations $c/\rho < 0.02$, where the minimum radius of curvature is around 20 mm and the clearance is below 0.4 mm.

Because β is small the assumption that the angles φ ($0 < \varphi < \beta$) and ξ ($\xi = \beta/2$, eq. C-9) would be small was valid.

Combination of eqs. C-4 and C-12 with the expression for the friction torque T_{fr}, caused by one couple of forces, gives:

$$T_{fr} = 2\, \mu\, F\, \frac{d}{2} = \frac{\mu d E I}{\rho\sqrt{6c\rho}} \tag{C-13}$$

where
d = the drive-shaft diameter
μ = the friction coefficient between drive-shaft and catheter-tube material

The rotation error angle θ over a shaft length l, which equals minus the torsion angle η due to this torque, is given by:

$$\theta = \psi_{dist} - \psi_{prox} = -\frac{T_{fr}\, l}{S_t} = -\frac{\mu d l E I}{S_t \rho\sqrt{6c\rho}} \tag{C-14}$$

and is negative, because the direction of the driving rotation angle ωt is chosen to be positive.

Case 2

In case a curved section of the catheter-tube ends at both sides in a straight piece of tubing, the situation changes (Fig. C-4).

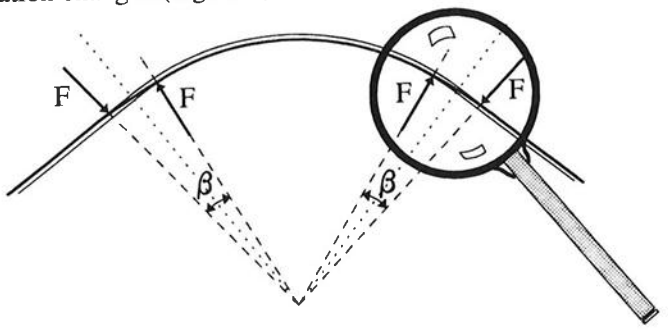

Fig. C-4 Curved section of a catheter-tube with straight ends and a drive-shaft inside.

In the straight sections of the tube, the shaft will also be straight if the clearance is small, so that here the bending moment is zero, which is the result of no external forces in these straight parts.
At the end of the curve, going into the straight part, the situation of external forces differs from the situation of case 1, but can be described analogously by substituting ρ_{ob}' for ρ_{ob} (Fig. C-5).

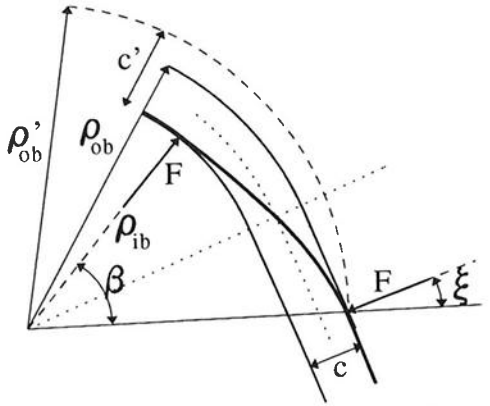

Fig. C-5 Detail of drive-shaft in curved catheter-tube with straight ends for $0 \leq \varphi \leq \beta$ (Fig. C-4), with definition of geometrical quantities.

So that we can define:

$$\rho' = \frac{\rho'_{ob} + \rho_{ib}}{2} \qquad \text{(C-15)}$$

$$c' = \rho'_{ob} - \rho_{ib} \tag{C-16}$$

and similar to eq. C-12 we find:

$$\frac{c'}{\rho'} = \frac{\beta^2}{6} \tag{C-17}$$

From Fig. C-5 we also find, combined with eq. C-9:

$$\rho'_{ob} = \frac{\rho_{ob}}{\cos\xi} \approx \frac{\rho_{ob}}{1 - \beta^2/8} \tag{C-18}$$

And we had defined earlier:

$$\begin{cases} \rho_{ob} = \rho + \dfrac{c}{2} \\ \rho_{ib} = \rho - \dfrac{c}{2} \end{cases} \tag{C-19}$$

Substitution of eqs. C-15 and C-16 in eq. C-17 and elimination of ρ_{ob}', ρ_{ob} and ρ_{ib}, using eqs. C-18 and C-19, gives:

$$\frac{c}{\rho} = \frac{8\beta^2 - 2\beta^4}{192 - 12\beta^2 - \beta^4} \tag{C-20}$$

Because β is small the higher order terms can be neglected so that we find:

$$\beta = 2\sqrt{\frac{6c}{\rho}} \tag{C-21}$$

The angle β partly covers the curved section and partly the straight section (Fig. C-5). The part covering the straight section equals the angle $\xi = \beta/2$, so that the transition from curved to straight tubing is situated halfway the angle β.

Combination of eqs. C-4 and C-21 with the expression for the friction torque T_{fr}, caused by <u>one</u> couple of forces, gives:

$$T_{fr} = 2\,\mu\,F\,\frac{d}{2} = \frac{\mu d E I}{2\rho\sqrt{6c\rho}} \tag{C-22}$$

The rotation error angle θ over a shaft length l, which equals minus the torsion angle η due to this torque, is given by:

$$\theta = \psi_{dist} - \psi_{prox} = -\frac{T_{fr}\,l}{S_t} = -\frac{\mu d l E I}{2 S_t \rho\sqrt{6c\rho}} \tag{C-23}$$

APPENDIX D Effect of $EI_{\bar{y}} \neq EI_{\bar{z}}$ and pre-curvature, combined with friction, on the rotation transmission characteristics of a flexible drive-shaft; analytical modelling

$EI_{\bar{y}} \neq EI_{\bar{z}}$ in combination with friction

The amplitude of the fluctuation of the driving torque due to unequal bending rigidity in different bending planes for a 90° curve is according to eqs. B-16 and B-19:

$$T_{EI,\max} = \frac{\pi p \overline{EI}}{2\rho_1} \tag{D-1}$$

For a curve with straight ends the driving torque due to friction (due to two couples of lateral forces) is according to eq. 4-20:

$$T_{fr} = \frac{\mu dEI}{\rho_1\sqrt{6c\rho_1}} = \frac{\mu dEI\kappa_1^{1.5}}{\sqrt{6c}} \tag{D-2}$$

where $\kappa_1 = 1/\rho_1$ is the catheter-tube curvature.

Theoretically this driving torque is constant, but in case of combination of $EI_{\bar{y}} \neq EI_{\bar{z}}$ and friction, the driving torque due to friction will receive a fluctuation synchronously with T_{EI} and with amplitude:

$$T_{fr,a} = \frac{\mu dp\overline{EI}}{\rho_1\sqrt{6c\rho_1}} \tag{D-3}$$

on a constant friction torque level of $T_{fr,c}$:

$$T_{fr,c} = \frac{\mu d\overline{EI}}{\rho_1\sqrt{6c\rho_1}} \tag{D-4}$$

The maximum driving torque due to $EI_y \neq EI_z$ can be compared with this amplitude of the torque due to friction by calculating:

$$\frac{T_{EI,\max}}{T_{fr,a}} = \frac{\pi\sqrt{6c\rho_1}}{2\mu d} \tag{D-5}$$

Choosing practical values for all parameters in this equation will show that $T_{fr,a}$ is at least one order of magnitude smaller than $T_{EI,max}$.
In case of this combination of influences the periodic error angle will therefore be mainly determined by the influence $EI_y \neq EI_z$.

The friction however may cause a significant off-set of the error angle because the value of

$$\frac{T_{EI,\max}}{T_{fr,c}} = \frac{\pi p\sqrt{6c\rho_1}}{2\mu d} \tag{D-6}$$

can easily be smaller than 10 for small enough p and ρ_1.

Pre-curvature in combination with friction

The amplitude of the fluctuation of the driving torque due to pre-curvature κ_0 of the drive-shaft (radius of curvature ρ_0) is for a 90° curve according to eq. B-32:

$$T_{\rho_0,\max} = \frac{\pi EI}{2\rho_0} = \frac{\pi EI\kappa_0}{2} \tag{D-7}$$

In case of combination of pre-curvature and friction, the driving torque due to friction will receive a fluctuation synchronously with $T_{\rho 0}$, with amplitude $T_{fr,a}$:

$$T_{fr,a} = \frac{\mu dEI}{2\sqrt{6c}}\{(\kappa_1 + \kappa_0)^{1.5} - (\kappa_1 - \kappa_0)^{1.5}\} \tag{D-8}$$

If $\kappa_1 >> \kappa_0$, then this equation can be simplified into:

$$T_{fr,a} \approx \frac{3\mu dEI}{2\sqrt{6c}}\kappa_0\sqrt{\kappa_1} \tag{D-9}$$

This fluctuation is added to the constant friction torque level $T_{fr,c}$:

$$T_{fr,c} = \frac{\mu d EI}{2\sqrt{6c}}\{(\kappa_1 + \kappa_0)^{1.5} + (\kappa_1 - \kappa_0)^{1.5}\} \qquad \text{(D-10)}$$

which under the same condition can be simplified into:

$$T_{fr,c} \approx \frac{\mu d EI}{\sqrt{6c}}\kappa_1\sqrt{\kappa_1} \qquad \text{(D-11)}$$

The maximum torque due to pre-curvature can be compared with this amplitude of the torque due to friction by calculating:

$$\frac{T_{\rho_0,max}}{T_{fr,a}} = \frac{\pi\kappa_0\sqrt{6c}}{\mu d\{(\kappa_1 + \kappa_0)^{1.5} - (\kappa_1 - \kappa_0)^{1.5}\}} \approx \frac{\pi\sqrt{6c}}{3\mu d\sqrt{\kappa_1}} = \frac{\pi\sqrt{6c\rho_1}}{3\mu d} \qquad \text{(D-12)}$$

Similar to eq. D-5 this ratio will be larger than 10 for practical values of all parameters, so that the effect of fluctuating friction due to pre-curvature can be neglected with respect to the effect of pre-curvature itself.
A relatively significant off-set of the error angle can be caused by the constant part of the friction torque when:

$$\frac{T_{\rho_0,max}}{T_{fr,c}} = \frac{\pi\kappa_0\sqrt{6c}}{\mu d\{(\kappa_1 + \kappa_0)^{1.5} + (\kappa_1 - \kappa_0)^{1.5}\}} \approx \frac{\pi\kappa_0\sqrt{6c}}{2\mu d\kappa_1\sqrt{\kappa_1}} = \frac{\pi\rho_1\sqrt{6c\rho_1}}{2\mu d\rho_0} \qquad \text{(D-13)}$$

is smaller than 10, which is the case for small enough κ_0 and large enough κ_1.

APPENDIX E Finite element model description

The catheter shaft is modelled by a string of spatial beam elements having two nodes at the ends. It is assumed that the catheter is clamped at one end while the shaft is driven by a motor at a constant angular velocity. The catheter shaft is confined within a tube with an inner diameter D_i which is larger than the outer diameter D_o of the string.
We shall describe the kinematic and dynamic modelling for the nodes, the elements and the interaction between the shaft and the wall, whereafter we describe the solution method for the resulting equations.

Kinematics

Nodes

The nodes have six degrees of freedom, three for the translations and three for the rotations. The translations are simply defined by the Cartesian coordinates of the nodes in a global coordinate system. The rotations are described by proper 3 × 3 rotation matrices R, i.e. matrices which are orthogonal, $R^T = R$, and have a determinant equal to one, det R = 1. The rotation matrix is split up as a product of a matrix which describes the initial orientation and three elementary rotation matrices for rotations about three axes. The rotation matrix which describes the initial orientation is built up from an orthogonal triad of unit vectors. The unit vector $\mathbf{n}_{x0}$ points along the central axis of the shaft and the other two, $\mathbf{n}_{y0}$ and $\mathbf{n}_{z0}$, are orthogonal to $\mathbf{n}_{x0}$; so the initial rotation matrix R_0 is:

$$R_0 = \begin{bmatrix} \mathbf{n}_{x0}^T \\ \mathbf{n}_{y0}^T \\ \mathbf{n}_{z0}^T \end{bmatrix}$$

An actual orientation of a node is given by the product of four matrices:

$$R = R_1 R_2 R_3 R_0$$

where

$$R_1 = \begin{bmatrix} 1 & 0 & 0 \\ 0 & \cos\varphi_1 & \sin\varphi_1 \\ 0 & -\sin\varphi_1 & \cos\varphi_1 \end{bmatrix}, \quad R_2 = \begin{bmatrix} \cos\varphi_2 & 0 & -\sin\varphi_2 \\ 0 & 1 & 0 \\ \sin\varphi_2 & 0 & \cos\varphi_2 \end{bmatrix}, \quad R_3 = \begin{bmatrix} \cos\varphi_3 & \sin\varphi_3 & 0 \\ -\sin\varphi_3 & \cos\varphi_3 & 0 \\ 0 & 0 & 1 \end{bmatrix}$$

The three generalized coordinates that describe the orientation are the three angles φ_1, φ_2 and φ_3, which are called modified Euler angles or Briant angles [1]. The choice of the order of rotations is based on the fact that φ_2 and φ_3 remain small, while φ_1 can become arbitrarily large, so there are no difficulties associated with singularities. In this way it is also easier to describe the interaction between shaft and tube, as will be seen later on.

Elements

The elements used were originally developed by Besseling (1974) in order to analyse the buckling and post-buckling behaviour of beam structures [2]. Later, Van der Werff and Jonker (1984) used the same element for dynamic purposes by adding a mass description [3]. The element used here is described by Meijaard (1991) [4].
The geometry of the element is defined by its two end-nodes p and q, which have the positions $\mathbf{x}^p$ and $\mathbf{x}^q$, and the orientations R^p and R^q. At the basis of the formulation of the element is the definition of so-called generalized deformations, which are invariant under finite translations and rigid body rotations. For the spatial beam element these generalized deformations are chosen to be:

$$\varepsilon_1 = \frac{l^2 - l_0^2}{2l_0} + \frac{1}{30l_0}(2\varepsilon_3^2 + \varepsilon_3\varepsilon_4 + 2\varepsilon_4^2 + 2\varepsilon_5^2 + \varepsilon_5\varepsilon_6 + 2\varepsilon_6^2)$$

$$\varepsilon_2 = \frac{l_0}{2}(\mathbf{n}_z^p.\mathbf{n}_y^q - \mathbf{n}_y^p.\mathbf{n}_z^q)$$

$$\varepsilon_3 = -\mathbf{n}_z^p \,.\, \mathbf{l}$$

$$\varepsilon_4 = \mathbf{n}_z^q \,.\, \mathbf{l}$$

$$\varepsilon_5 = \mathbf{n}_y^p \,.\, \mathbf{l}$$

$$\varepsilon_6 = -\mathbf{n}_y^q \,.\, \mathbf{l}$$

where

$$\mathbf{l} = \mathbf{x}^q - \mathbf{x}^p \quad , \quad l = \|\mathbf{l}\|$$

and l_0 is the initial undeformed length of the element.

The initial geometry of the structure is defined by the Cartesian coordinates of the nodes and unit vectors in the direction of the central axis of the shaft at the nodes. The orientation matrix of the first node is defined in such a way that the vector $\mathbf{n}_{x0}$ is pointing

in the direction of the central axis of the shaft and $\mathbf{n}_{y0}$ is in the global xy-plane. The initial orientation matrices of the next nodal points are calculated such that $\mathbf{n}_{x0}$ points along the central axis of the shaft and the torsional deformation ε_2 is zero. The initial length is calculated from the requirement that initially the elongation ε_1 is zero. After this initialization, the generalized deformations can be calculated from the positions and orientations of the nodal points for any given displacements.

Interaction between the shaft and the catheter-tube wall

The intrusion of the shaft in the tube wall and the relative speeds in the contact areas are calculated in the nodal points and in points in the middle of the elements, which are treated as sample points for the interaction. In the initial position, the coordinates $\mathbf{x}_{m0}$ and the direction of the shaft central axis $\mathbf{n}_{xm0}$ at the middle points are defined as follows [4, eq. 12]:

$$\mathbf{x}_{m0} = \frac{1}{2}(\mathbf{x}^p + \mathbf{x}^q) + \frac{1}{8}(\varepsilon_3\mathbf{n}_z^p + \varepsilon_4\mathbf{n}_z^q - \varepsilon_5\mathbf{n}_y^p - \varepsilon_6\mathbf{n}_y^q)$$

$$\alpha\mathbf{n}_{xm0} = (\mathbf{x}^q - \mathbf{x}^p) + \frac{1}{4}(-\varepsilon_3\mathbf{n}_z^p + \varepsilon_4\mathbf{n}_z^q + \varepsilon_5\mathbf{n}_y^p - \varepsilon_6\mathbf{n}_y^q)$$

The positive factor α is chosen in such a way that $\mathbf{n}_{xm0}$ is a unit vector. The radial displacement is given by:

$$r = \|\mathbf{x} - \mathbf{x}_0 - \mathbf{n}_{x0}(\mathbf{x} - \mathbf{x}_0).\mathbf{n}_{x0}\|$$

If the radial displacement is not zero, three directions are defined in each sample point, an axial, normal and tangential direction:

$$\mathbf{n}_a = \mathbf{n}_{x0} \; ; \quad \alpha\mathbf{n}_r = \mathbf{x} - \mathbf{x}_0 - \mathbf{n}_{x0}(\mathbf{x} - \mathbf{x}_0).\mathbf{n}_{x0} \; ; \quad \mathbf{n}_t = \mathbf{n}_a \times \mathbf{n}_r$$

The normal velocity v_r and the tangential velocity v_t at the contact point are given by $r_o = D_o/2$:

$$v_r = \mathbf{v}.\mathbf{n}_r \; ; \quad v_t = \mathbf{v}.\mathbf{n}_t + \dot{\varphi}_1 r_o$$

Dynamics

Nodes

At the nodes, lumped masses can be added. These masses can represent some device attached to the node or a rotational inertia of a disk at a node, as a correction for the finite cross-sectional dimensions of the shaft. The kinetic energy of the lumped mass m and the disk with I_{xx}, $I_{yy} = 0.5\ I_{xx}$, $I_{zz} = 0.5I_{xx}$ and $I_{xy} = I_{xz} = I_{yz} = 0$ is:

$$T_{Node} = \frac{1}{2}m(\dot{x}_1^2+\dot{x}_2^2+\dot{x}_3^2) +$$
$$\frac{1}{4}I_{xx}[2(\dot{\varphi}_1-\sin\varphi_2\dot{\varphi}_3)^2 + (\cos\varphi_1\dot{\varphi}_2+\sin\varphi_1\cos\varphi_2\dot{\varphi}_3)^2 + (-\sin\varphi_1\dot{\varphi}_2+\cos\varphi_1\cos\varphi_2\dot{\varphi}_3)^2]$$

The contributions to the global mass matrix and force vector are given by:

$$\mathbf{M} = \begin{bmatrix} m & 0 & 0 & 0 & 0 & 0 \\ 0 & m & 0 & 0 & 0 & 0 \\ 0 & 0 & m & 0 & 0 & 0 \\ 0 & 0 & 0 & I_{xx} & 0 & -I_{xx}\sin\varphi_2 \\ 0 & 0 & 0 & 0 & \frac{1}{2}I_{xx} & 0 \\ 0 & 0 & 0 & -I_{xx}\sin\varphi_2 & 0 & \frac{1}{2}I_{xx}(1+\sin^2\varphi_2) \end{bmatrix}; \quad \mathbf{f} = \begin{bmatrix} 0 \\ 0 \\ 0 \\ I_{xx}\cos\varphi_2\dot{\varphi}_2\dot{\varphi}_3 \\ I_{xx}\cos\varphi_2\dot{\varphi}_3(-\dot{\varphi}_1+\frac{1}{2}\sin\varphi_2\dot{\varphi}_3) \\ I_{xx}\cos\varphi_2\dot{\varphi}_2(\dot{\varphi}_1-\sin\varphi_2\dot{\varphi}_3) \end{bmatrix}$$

External forces and moments, such as gravitation, are represented by concentrated forces and moments in the nodes.

Elements

The element mass matrix and velocity dependent inertia force vector are given by Meijaard [4]:

$$\mathbf{M}^e = \frac{m^e l_0^e}{420}\begin{bmatrix} 156\mathrm{I} & 22l_0^e\mathrm{A} & 54\mathrm{I} & -13l_0^e\mathrm{B} \\ & 4l_0^{e2}\mathrm{A}^T\mathrm{A} & 13l_0^e\mathrm{A}^T & -3l_0^{e2}\mathrm{A}^T\mathrm{B} \\ & & 156\mathrm{I} & -22l_0^e\mathrm{B} \\ & & & 4l_0^{e2}\mathrm{B}^T\mathrm{B} \\ \text{symm.} & & & \end{bmatrix}$$

$$-\mathbf{f}_{in}^e = \frac{m^e l_0^e}{420}\begin{bmatrix} l_0^e(22\mathrm{A}'\dot{\phi}^p\dot{\phi}^p-13\mathrm{B}'\dot{\phi}^q\dot{\phi}^q) \\ l_0^{e2}(4\mathrm{A}^T\mathrm{A}'\dot{\phi}^p\dot{\phi}^p-3\mathrm{A}^T\mathrm{B}'\dot{\phi}^q\dot{\phi}^q) \\ l_0^e(13\mathrm{A}'\dot{\phi}^p\dot{\phi}^p-22\mathrm{B}'\dot{\phi}^q\dot{\phi}^q) \\ l_0^{e2}(-3\mathrm{B}^T\mathrm{A}'\dot{\phi}^p\dot{\phi}^p+4\mathrm{B}^T\mathrm{B}'\dot{\phi}^q\dot{\phi}^q) \end{bmatrix}$$

where

$$A = \frac{\partial(R^p \mathbf{n}_x^p)}{\partial \varphi^p}, \quad B = \frac{\partial(R^q \mathbf{n}_x^q)}{\partial \varphi^q}, \quad A' = \frac{\partial A}{\partial \varphi^p}, \quad B' = \frac{\partial B}{\partial \varphi^q}$$

Forces due to gravitation are represented by concentrated forces at the nodes and the middle points of the elements.

The stiffness and damping properties of the elements are given by a Kelvin-Voigt model which yields a linear relation between the generalized element stresses and the strains and strain rates as [6]:

$$\sigma^e = S(\varepsilon^e - \varepsilon_0^e) + S_d \dot{\varepsilon}^e$$

where ε_0^e are the initial deformations and

$$S = \begin{bmatrix} S_1 & 0 & 0 & 0 & 0 & 0 \\ 0 & S_2 & 0 & 0 & 0 & 0 \\ 0 & 0 & 4S_3 & -2S_3 & 0 & 0 \\ 0 & 0 & -2S_3 & 4S_3 & 0 & 0 \\ 0 & 0 & 0 & 0 & 4S_4 & -2S_4 \\ 0 & 0 & 0 & 0 & -2S_4 & 4S_4 \end{bmatrix}, \quad S_1 = \frac{EA}{l_0^e}, \quad S_2 = \frac{S_t}{l_0^{e3}}, \quad S_3 = \frac{EI_{\bar{y}}}{l_0^{e3}}, \quad S_4 = \frac{EI_{\bar{z}}}{l_0^{e3}},$$

$$S_d = \begin{bmatrix} S_{d1}S_1 & 0 & 0 & 0 & 0 & 0 \\ 0 & S_{d2}S_2 & 0 & 0 & 0 & 0 \\ 0 & 0 & 4S_{d3}S_3 & -2S_{d3}S_3 & 0 & 0 \\ 0 & 0 & -2S_{d3}S_3 & 4S_{d3}S_3 & 0 & 0 \\ 0 & 0 & 0 & 0 & 4S_{d4}S_4 & -2S_{d4}S_4 \\ 0 & 0 & 0 & 0 & -2S_{d4}S_4 & 4S_{d4}S_4 \end{bmatrix}$$

Interaction between the shaft and the catheter-tube wall

In normal direction, the radial restoring force per unit of length of the shaft f_r depends on the radial displacement r and the radial velocity v_r. For three regions of radial displacements, three force laws are defined ($\xi = (r+r_0-r_a)/(r_b-r_a)$):

$$r \le r_a - r_0: \qquad f_r = 0$$

$$r_a - r_0 < r < r_b - r_0: \quad f_r = -k_w(r_b - r_a)\xi^3(1 - \xi/2) - c_w v_r \xi^3(10 - 15\xi + 6\xi^2)$$

$$r > r_b - r_0: \qquad f_r = -k_w(r_b - r_a)(\xi - \tfrac{1}{2}) - c_w v_r$$

If the value of f_r as given above is positive, it is replaced by zero. The tangential force per unit of length f_t is given by a Coulomb-type friction law which is smoothed at $v_t = 0$:

$$f_t = \mu \arctan(k_\mu v_t)\frac{2}{\pi} f_r$$

This results in a total nodal force per unit of length of:

$$\mathbf{f} = f_t \mathbf{n}_t + f_r \mathbf{n}_r + m^e \mathbf{g} - c\mathbf{v}$$

where c is a damping coefficient, and a torsion moment per unit of length:

$$M_1 = f_t r_o$$

The total forces and moments at the nodes are obtained by multiplying the values per unit of length with a part of the length of the element. For the middle nodes, this part is taken as two thirds of the element length and for the end-nodes this part is taken as the sum of one sixth of the element length of the elements at each side of the node. This choice is based on the well-known integration method of Simpson.

Equations of motion

The forces in the middle points of the elements are replaced by equivalent nodal forces as:

$$\mathbf{f}_{eq}^{p,q} = \begin{bmatrix} (\partial \mathbf{x}_m / \partial \mathbf{x}^{p,q})^T \mathbf{f}_m \\ \frac{1}{2} M_{m1} \\ 0 \\ 0 \end{bmatrix}$$

By assembling the global mass matrix M and force vector **f**, the equations of motion for the entire system become:

$$\mathbf{M}\ddot{\mathbf{x}} = \mathbf{f}, \quad \ddot{\mathbf{x}} = \mathbf{M}^{-1}\mathbf{f}$$